



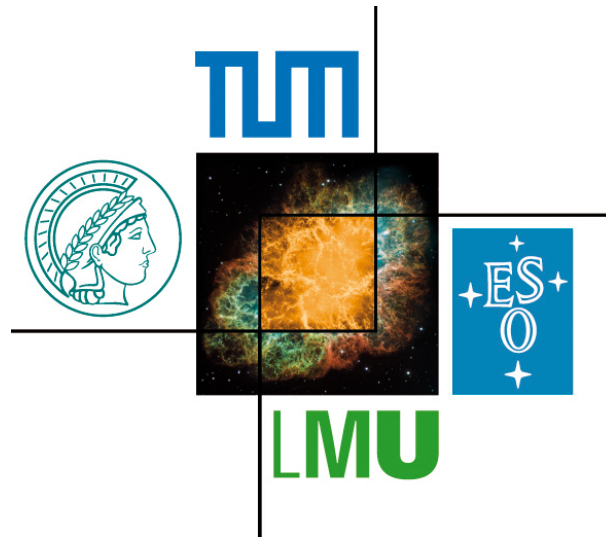
Abschlussarbeit im Bachelorstudiengang Physik

Untersuchungen zu Entladungswahrscheinlichkeiten eines auf GEM basierten Detektors

Discharge probability studies on single-GEM detector

Jennifer Lisa Padberg

16. September 2015



Erstgutachter (Themensteller): Prof. L. Fabbietti
Zweitgutachter: Dr. A. Ulrich

Betreuer: Dr. P. Gasik

Contents

Introduction	v
1 Principles of a GEM TPC	1
1.1 Time Projection Chamber	1
1.2 The ALICE – TPC	3
1.3 GEM - Gas Electron Multiplier	4
2 Detector Design	9
2.1 Solid Works and laboratory preparations	9
2.2 Dimensions and main interiority of the detector	10
2.3 Characteristics of the field cage	13
3 Detector commissioning	15
3.1 HV settings	15
3.2 Readout system	16
3.3 Gas mixture	17
3.4 Sources	18
3.5 Rate determination	18
3.6 Energy resolution (ER)	20
4 Gain measurement	21
4.1 Definition	21
4.2 Gain calculations and error estimation	22
5 Discharge studies	25
5.1 Definition	25
5.2 Results and comparison to the TDR addendum	25
6 Summary & Outlook	29
6.1 Summary	29
6.2 Outlook	29
A Oscilloscope signals	31
Bibliography	33

Contents

Acknowledgements 35

Introduction

ALICE is the acronym for **A Large Ion Collider Experiment**. It is part of the **Large Hadron Collider (LHC)** in the major research facility CERN near Geneva. With about 2.400 employees, it is one of the largest current single experiments. ALICE is optimized to study heavy-ion (Pb-Pb nuclei) collisions with a resulting temperature and energy density, which are expected to be high enough to produce quark-gluon plasma.

QGP is the state of matter, described by Quantum Chromodynamics (QCD) in the standard model of particle physics, wherein quarks and gluons are freed. Similar conditions are believed to have existed a fraction of the second after the Big Bang where quarks and gluons existed in a weakly interacting state before they bound together to form Hadrons and heavier particles. According to the valence quarks of which they are composed, hadrons can be classified: mesons, made of a quark-antiquark pair, and baryons, made of three quarks. [1]

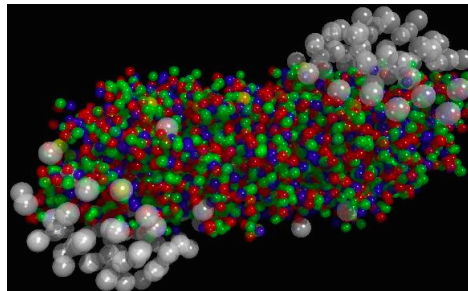


Figure 1: Schematic sketch of quark-gluon plasma with an extra charge, the color (red, green, blue and their three corresponding negative values) [2]

The existence of the quark-gluon plasma and its properties are key issues in Quantum Chromodynamics for understanding color confinement and chiral symmetry restoration. ALICE is equipped with optimized tracking systems in order to be able to analyze and reconstruct such high energy densities. The main central tracking device of the ALICE experiment is the **Time Projection Chamber (TPC)**. Up to now the TPC uses gated **Multi Wire Proportional Chambers (MWPCs)** with pad

readout to amplify and read out the signal. The gate consists of an array of wires that collects the ions produced in the amplification process, to detain them from drifting back in the drift volume, which would contingently lead to variances of the electron trajectories and thus to distortions of the reconstructed tracks.

Currently the maximum readout rate of the TPC is ~ 300 Hz due to their low velocity ($v_{ion} \sim 10^{-3} v_e$). [3] This rate is much lower than the maximum collision rate required for RUN 3 (50 kHz) which will take place beyond 2019. To fulfill the new requirements the ALICE experiment is planning a major upgrade of the TPC for the upcoming RUN 3 at LHC. To estimate the conditions under a GEM based detector, a first prototype of a GEM based TPC **I**nner **R**ead **O**ut **C**hamber (IROC) has been built and tested at the Technische Universität München.

It occurred that the most problematic requirements associated to the LHC environment, chiefly in the high multiplicity scenario of Pb-Pb collisions, is the stability against electric discharges. The stability against sparks arise by high charge densities on the GEM foils.

The aim of this bachelor thesis is to study the gain and discharge probability. Therefore a new design of a GEM based detector is introduced with a new component, the field cage which is intended to homogenize the electric field. Furthermore it presents the results obtained in the laboratories.

Chapter 1

Principles of a GEM TPC

The principle of gaseous detectors are based on the straight assemblage of the ionization electrons produced by a charged particle passing through the gas medium. The TPC is the main charged particle ID and tracking device of ALICE.

1.1 Time Projection Chamber

A time projection chamber is a particle detector which consists a gas filled detection volume in a homogenous electric field. The most common design is a cylindrical chamber with a beam pipe going through the rotation axis of the TPC with the interaction point at its center.

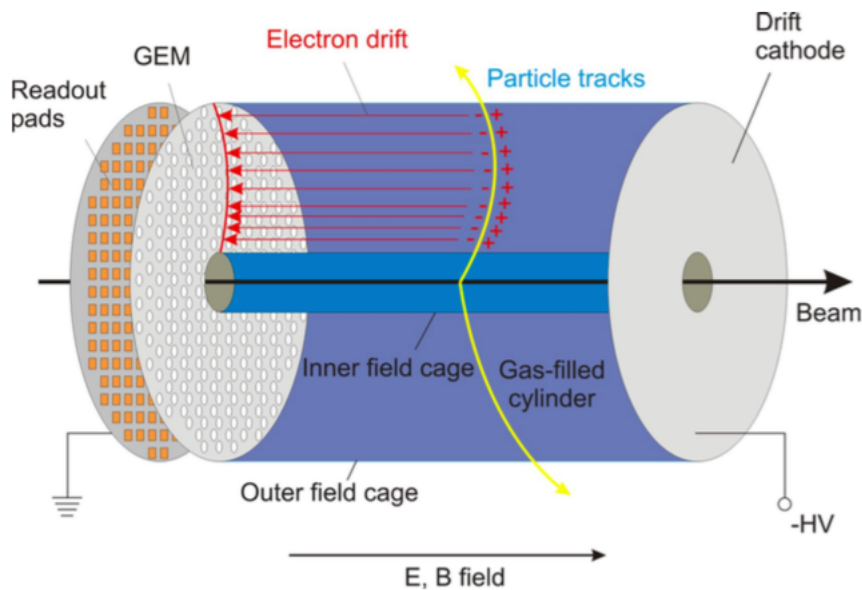


Figure 1.1: General schematics of a TPC with GEM based design [4]

The cathode (placed in the center or on the one end of the TPC) is at a high potential whereas the anode is at ground potential which results in a drift field between these two electrodes. The TPC is a so called 4π detector which covers nearly the whole solid angle. The basic idea of the measurement principle is a charged particle traversing the gas volume of the TPC ionizing the atoms of the gas mixture which consists of 90% noble gas and 10% quencher gas. [5] The released electrons drift in the electric field which is applied between the end plates of the chamber towards the anode. [6] To be able to measure the position of the particle trajectory as accurately as possible, the electric field has to be very homogeneous around the drift volume of the TPC. This can be achieved by a field cage, which usually consists of conducting strips around the cylinder. These strips divide the potential from the cathode stepwise down to the anode. Additionally, a high magnetic field parallel to the electric field is used to bend the trajectory of the particle on a spiral track due to the Lorentz force. This gives the possibility to calculate the momentum of the particle from the knowledge of the bend and the B-field. At the anode plane, the electrons can be detected on the readout plane which is segmented in the directions perpendicular to the drift direction. As the electron signal from the primary ionization process is only of the order of 100 electrons per centimeter, the signal needs to be amplified before being detectable.

Conventionally this has been done with Multi Wire Proportional Chambers [7] or, in the future, with Gas Electron Multipliers (GEMs). The r - Φ position (coordinates perpendicular to the cylinder axis) of the trajectory can be reconstructed directly from the coordinates of its projection on the pad plane. The z position (coordinate along the cylinder axis) is reconstructed from the drift time (time between particle passing the TPC volume and measured signal on the pads) and the electron drift velocity measured for the gas mixture used in a TPC. Therefore an external timing information, e.g. from a silicon detector, is needed. [8] These two measurements allow a full reconstruction of the track. Full particle identification (PID) can be done in a TPC by using both information, the dE/dx and momentum measurements in the magnetic field.

1.2 The ALICE – TPC

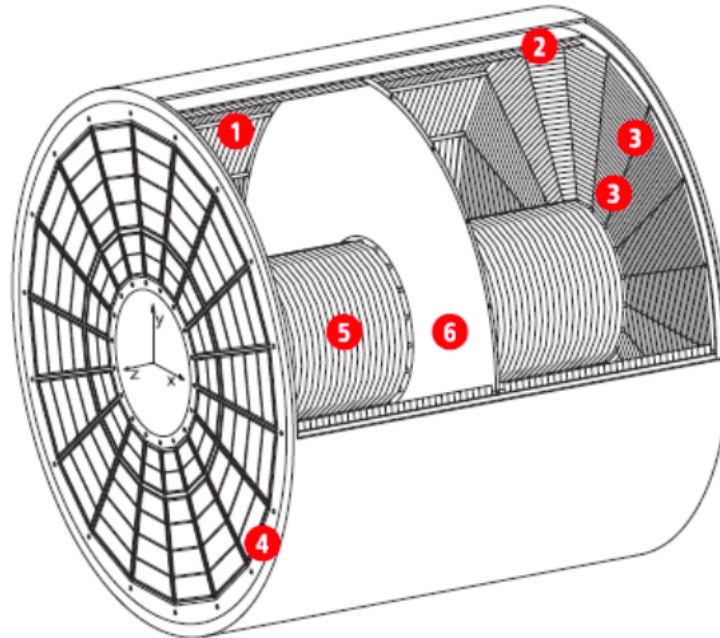


Figure 1.2: Schematic sketch of the time projection chamber of the ALICE experiment with the corresponding components. The outer and inner field cage (1, 5) is designed to provide a highly uniform electric field between the central HV electrode (6) and the readout wire chambers (3). The signal will be read out by the end plate (4). (2) shows the CO₂ – gap. [9]

The ALICE TPC is a large cylindrical volume filled with gas and divided in two drift regions by the central electrode located at its axial center. The TPC covers a total length of $-250\text{cm} < z < 250\text{cm}$. [10] The field cage ensures the uniform electric field along the z-axis. Charged particles traversing the TPC volume ionize the gas along their lane, releasing electrons that drift towards the end plates of the barrel.

The necessary signal amplification is provided through an avalanche effect in the locality of the anode wires looped in the readout. The readout of the signal is done by the pads that form the cathode plane of the multi-wire proportional chambers located at the TPC end plates. The readout chambers were specially designed to handle with the high track density expected in heavy ion collisions at LHC. The design of the field cage of the ALICE TPC is based on a novel construction principle

to adjust the detector to the specific running conditions with heavy ion collisions. The expected high particle densities make it necessary that the field cage keeps errors at a minimum in order not to impair the sensitive pattern recognition and resolution capabilities of the detector as a whole. Separated by the central HV electrode, the field cage has two detection volumes with an inner/outer diameter of 1.2/5 m and a drift length of 2.5 m each. [10]

The total sensitive detector volume is 88 m³, filled with a gas mixture of Ne-CO₂ with a proportion of 90-10 (in RUN 1 of the LHC) or Ar-CO₂ in the same proportions (in a current RUN2). With a drift field of 400 V/cm, this gas represents the optimum in terms of charge transport (velocity and diffusion), signal amplification and transparency for traversing particles. Hence, the field cage will have to sustain a maximum potential of 100 kV at its central electrode. Another unique feature of the field cage is its potential defining system designed to provide a uniform electric field among radial distortion. [9]

1.3 GEM - Gas Electron Multiplier

The GEM (Gas Electron Multiplier) has been invented by F. Sauli in 1996 and provides the possibility to avoid the main disadvantages of the Multi Wire Proportional Chambers. [11]

1.3.1 Disadvantages of the MWPCs

Traditionally, MWPCs have been used in TPC as standard device for gas amplification. To briefly introduce the functionality of MWPCs, tense parallel wires are mounted in front of the pad plane. By applying a high voltage to the wires, the emerging electric field accelerates the electrons. It can increase the energy of the primary electrons so they are able to ionize the gas. To level off the field towards the chamber and therefore to minimize the influence of the sense, an additional layer of wires are installed in this direction.

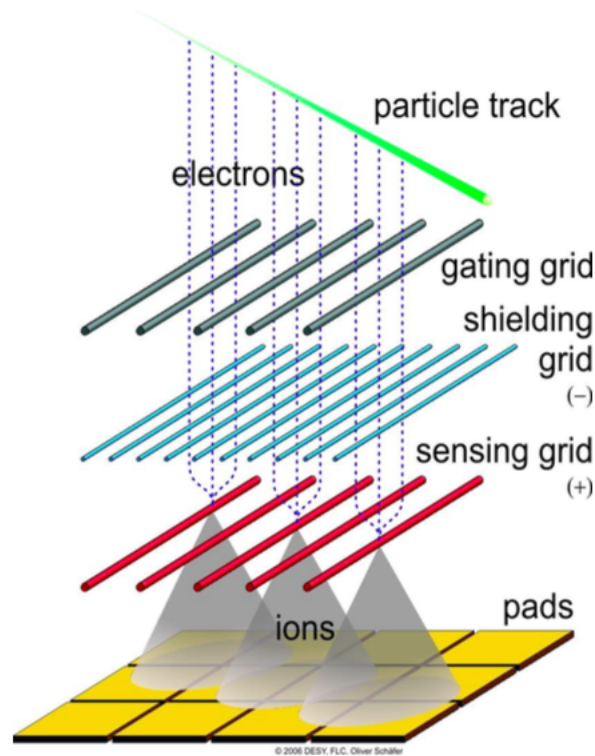


Figure 1.3: Layout of gas amplification and read-out with proportional wires. [8]

By drifting back to the TPC volume the produced ions induce a very broad signal on the pad plane behind the wires. The signal caused by the electrons is measured at the wires. Since the absence of ions in the TPC volume is favored, a third layer of wires which is called the gate is necessary. When the gate is open the gating wires are at the same potential as the field in this vicinity. At this instant, drifting electrons but also ions pass the grid without disturbance. To vacuum off the ions the grid has to be closed for some finite time limit. At this setting, the potential of neighboring wires is set altering to $\pm 50 - 100$ V. The drifting ions and electrons are collected on the wires.

This technique gives disadvantages, e.g. dead time to purge the TPC volume or the mechanically limited distance between two wires. This makes it difficult to separate two nearby tracks and set limits to the $r\Phi$ and tie resolution. A second disadvantage is the very high tension under the wires have to be mounted to provide a perfectly parallel alignment. Third, gating becomes impossible if the events do overlap which means the drift time is longer than the time between two events. [12] [13]

1.3.2 Principles of the GEM

GEMs are constructed of thin polyimide layers ($\sim 50 \mu\text{m}$) coated with copper layers ($\sim 5 \mu\text{m}$) on both sides. The foil undergoes a photolithographic process in which a dense and regular pattern of holes is etched. The holes which are usually double conical have an inner radius of $\sim 50 \mu\text{m}$ and an outer one of $\sim 70 \mu\text{m}$. Due to photolithographic methods they are densely etched so that the holes form a hexagonal pattern. The distance between two holes is $\sim 140 \mu\text{m}$. [14]

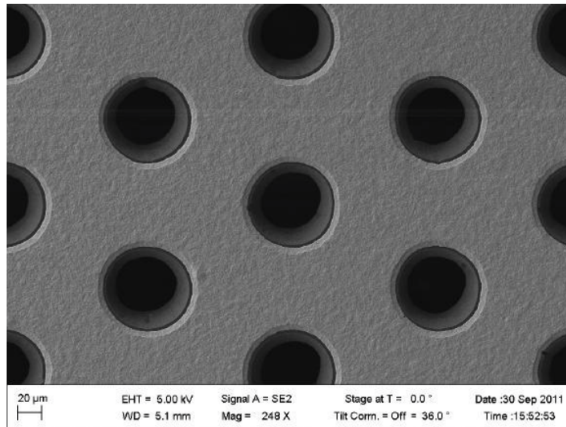


Figure 1.4: Standard GEM photographed with an electron microscope [15]

A strong electric field of $\mathcal{O}(50 \text{ kV})$ is created within a hole by applying a moderate potential difference of $\mathcal{O}(500 \text{ V})$ between the two conductive sides of the GEM. At the center of the holes the electric field lines are focused due to the double conical shape of the holes. Electrons passing the hole are producing an avalanche. One part of the electrons are collected on the bottom side of the GEM and the rest depending on the setup either drift towards the readout anode or the next amplification stage, in a multiple GEM stack.

The positive equivalent form the ions produced in the amplification. They are partially collected on the upper copper layer and partially drift back. A unique characteristic of GEMs is the intrinsic ion backflow.

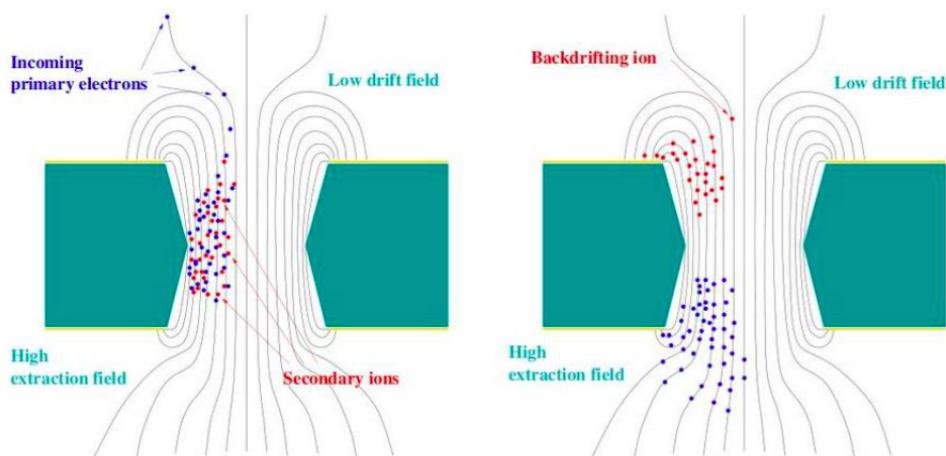


Figure 1.5: Working principle of a GEM: (left) electrons drift into a hole and create an avalanche, (right): most of the ions get absorbed at the top side of the GEM [16]

The first well working experiment using the technology based on GEMs was the COMPASS experiment at CERN [17] which developed triple GEM tracking detectors with parallel plate geometry. They achieved high efficiency (97%), good space-time resolution ($70 \mu\text{m}$, 12 ns) and a stability up to rates of $25 \text{ kHz}/\text{mm}^2$. [18] The GEM TPC prototype [19] developed for the PANDA experiment [20] is the most remarkable example for the ALICE experiment. The detector was successfully operated as a part of the FOPI spectrometer in GSI/Darmstadt. They used a $1.7 \text{ GeV}/c$ polarized pion beam colliding on a carbon target with a rate of $\sim 1.5 \times 10^4 \text{ Hz}$. The GEM detector operated at a gain of 3800.

1.3.3 Discharges

One disadvantage of GEMs is that they are quite fragile and can be damaged by discharges. Under present situations GEMs have to operate at extreme conditions when the discharge can appear with increased probability, e.g. at very high counting rates or in presence of heavily ionizing particles and high gas gain. [21] Discharges can also occur if the GEM presents microdefects, e.g. sharp edges, dirty spots or microparticles obstructing inside and outside of a hole which can be conductive. In the case of a good quality the Raether limit gives the physical limit for the gain in parallel plate detectors. [22] According to discharges are very likely to appear for a critical total charge of $\sim 10^7$ - 10^7 electrons. Due to simulations and experimental results a similar situation is expected for GEM detectors that a discharge occurs when the total charge in the avalanche reaches a critical value: $Q_{crit} \sim 10^6 - 10^7$

electrons [23] In double or triple GEM structures the electron density expands due to the enhanced diffusion. This results in a lower charge quantity and decreases the discharge probability but also allows higher gains in multiple GEM stacks compared to single GEMs. [24] In figure 1.6 a burned hole of the GEM foil induced by electric sparks is shown. This foil had to be removed from the detector since the foil was completely damaged.

This thesis deals with a systematic study of the discharge properties of a single GEM detector. The experimental results will be compared to the data taken from the Technical Design Report (TDR) of the ALICE collaboration. [25] The advantage of measuring the stability of the simplest configuration, including only one GEM foil, the intrinsic stability of the GEM foil against electrical discharges is completely uncoupled from the influence of other effects. In multi-GEM structures can occur other effects that has an influence on discharge probability, for example charge produced by electrons can be shared or spread between foils. [25]

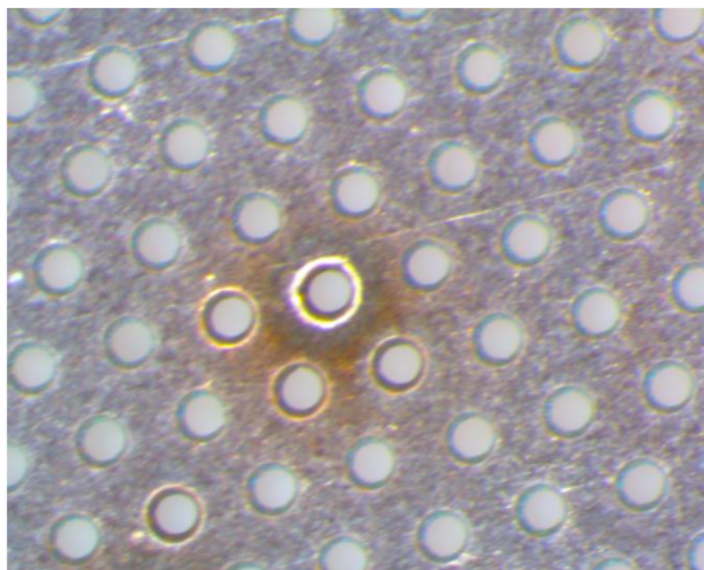


Figure 1.6: Burned hole of a GEM caused by a discharge

Chapter 2

Detector Design

The following chapter explains the design and dimensions of the detector which was used to measure gain and discharge probability. Furthermore it presents the detailed structure of the field cage with calculating its resistor chain.

2.1 Solid Works and laboratory preparations

Solid works is a solid modeling computer - aided design program. It is produced by the Dassault Systemes, S. A. since 1997 [26] . Solid works is a solid modeler and utilizes a parametric feature based approach. It is used to create models and assemblies.

The detector used for the experiment has been designed in solid works. (see fig. 2.1) The detector housing comprises the GEM holder, the field cage, the drift cathode and the readout anode. Giving a high flexibility to the whole setup the gas vessel and the GEM detector is separated. Moreover the detector box becomes gas tight by adding a rubber O-ring in the cap of the detector.

Machining holes, directly above the active stack and in the walls of the housing in alignment with the active volume, make it possible to shoot with a radiation source either from above or from the side into the drift volume. All windows of the detector box are completely sealed with a thin aluminized Mylar foil foil to hold it tight. Different holes were drilled into the box at the TUM workshop to merge the gas pipes, high voltage, the signal readout and the last strip of the field cage (see 2.3) connector. To avoid any dust, water or oxygen in the active volume the connectors had to be mounted gas tight. Due to this the gas tightness was checked before and during every single measurement to guarantee the accuracy of results. Avoiding a high oxygen content is necessary since oxygen molecules are very electronegative and thus would capture electrons to form ions. Dust content would increase the probability of electric sparks. The oxygen is measured using an oxygen meter connected to the gas output of the detector. The oxygen content saturated between 60 - 70 ppm for a gas flux of 10 l/h Ar - CO₂ (90-10).

To determine the pressure and temperature, which have a significant influence on

gain measurements, a so called weather station is installed in the GEM lab. These two values were verified before every measurement as well.

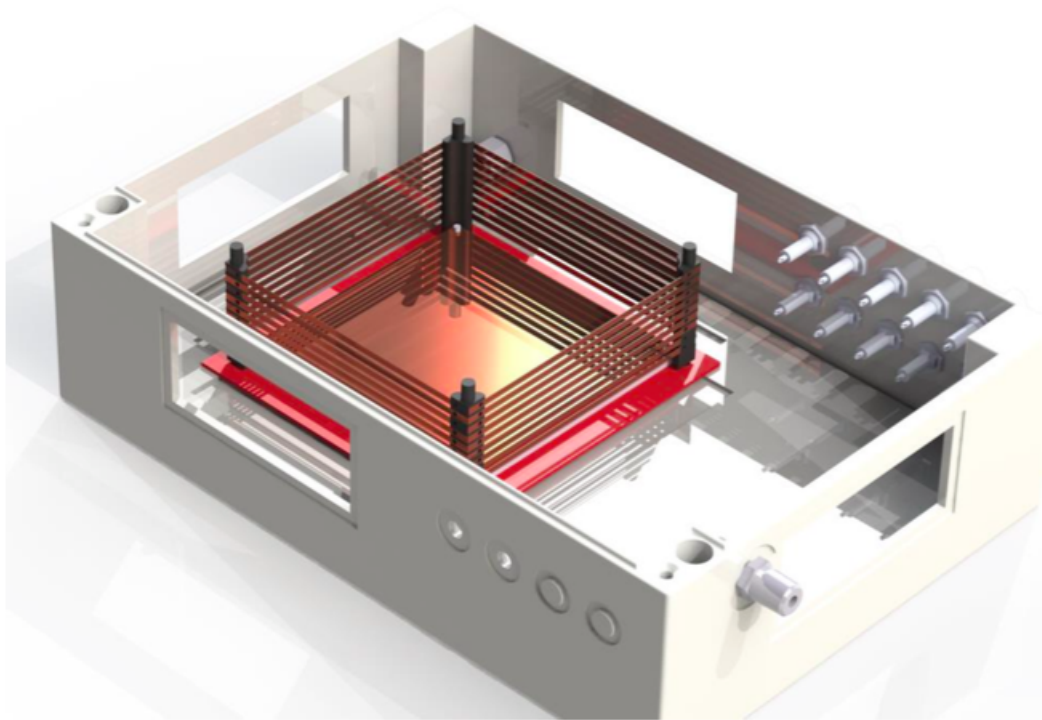


Figure 2.1: Detector drawing done by solid works with implemented field cage, GEM and anode

2.2 Dimensions and main interiority of the detector

For this detector setup a $10 \times 10 \text{ cm}^2$ GEM foil was used for amplification. Before mounting a foil in the detector it has to be checked. This includes a high voltage test to get information about the quality of the GEM concerning the amount of discharges and the leakage current. The quality of the GEM foil used for the measurements was very good since only one electric discharge occurred during the high voltage test and the leakage current was very low (0.5 nA). Second, the foil has to be stretched and framed to avoid any bending during the operation with high electric field. Third, a second high voltage test is necessary to exclude damage caused by framing. Testing

the GEM foil used for the measurements showed that no damage arised. A positive side effect off gluing foils on frames is the ability to mount GEMs together on a stack with defined gaps between them. The thickness of the frames determine the size of the so called transfer gap. To keep the possibility open to measure with multi GEM structure the detector was designed to variate the height of the field cage. Therefore more than one GEM foil can be assembled in the detector remaining the gap between the supreme foil and the last strip of the field cage the same. Within the scope of this work a GEM stack, consisting a single foil, was used. It is important to mention that a loading resistor of $10\text{ M}\Omega$ was soldered in series between GEM top and high voltage connector thus large currents are prevented, that can occur during a discharge and can damage the foil. In figure 2.2 a framed foil surrounded by the field cage is shown.

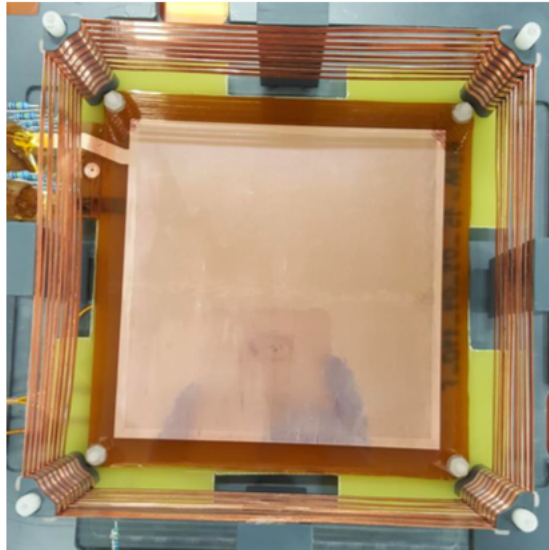


Figure 2.2: In the middle: GEM after high voltage test, stretched and glued on a frame. At the outer: Field cage strips mounted on the specific shaped pillars

The distance between the anode and the GEM foil, the so called induction gap, is 2 mm. The gap between the last strip of the field cage and the GEM foil is 3 mm just like the gap between cathode and first strip. The distance between two batched strips is 4.5 mm. The hole schematic sketch of the detector is shown in figure 2.3. As a whole the field cage was built of nine strips, covering an active plane of $135 \times 135\text{ cm}^2$, giving it a total height of 40.5 mm.

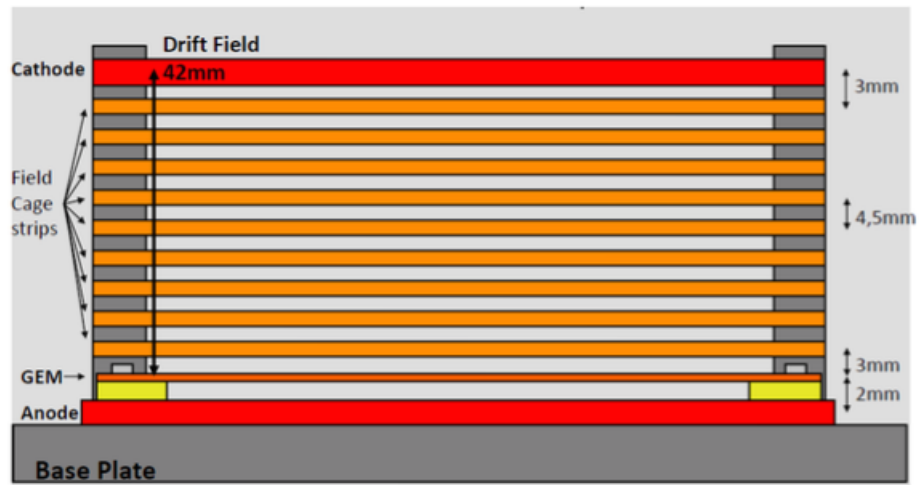


Figure 2.3: Schematic sketch of the prototype TPC detector with single GEM stack inside.

Both the cathode and the anode were made of a 1.5 mm thick PCB covered one side with a thin copper layer. The cathode which was used in the experiment was designed to perfectly match the dimension of the field cage to keep electric field distortions at a minimum. A 8 mm diameter hole located at the center of the cathode plate allows irradiation with a radioactive source perpendicular to the GEM plane. The schematic sketch of the cathode is shown in figure 2.4. The copper layer of the readout anode is segmented in three areas. The outer one is grounded, while the inner areas can be read out individually or together. The area of the small inner square amounts $2 \times 2 \text{ cm}^2$ and the middle square $8 \times 8 \text{ cm}^2$. The whole interiority of the detector mentioned up to now was soldered with their associated connector by a Kapton isolated wire.

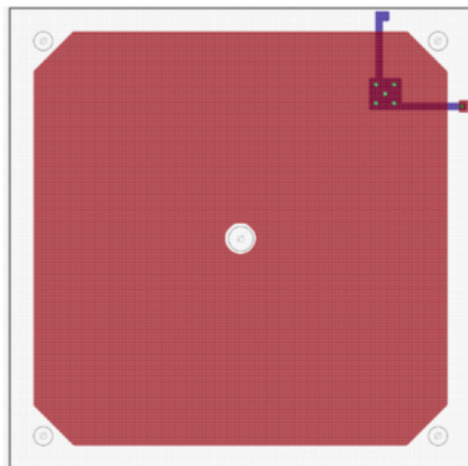


Figure 2.4: Drawing of the cathode with characteristic irradiation hole and specific copper layer

2.3 Characteristics of the field cage

Four pillars giving the foundation of the field cage were mounted at the edges of a squared shape. Nine 1mm thin strips composed of copper were screwed on the pillars. The shape of the pillars was designed to minimize electric field distortion furthermore they are covered with thin copper tape with the same width as the stripes. The tapes in addition to the specific shape of the pillars create a perfectly homogenous electric field even in the critical edges. (see fig. 2.2)

It is done by connecting the first strip to the cathode and the other strips together with suitable resistors to divide the potential from the cathode stepwise down to the GEM level. In this way, there is at any height of the drift field the perfectly matching potential. These resistors have been calculated by using the formula:

$$R = \frac{U}{I} \quad (2.1)$$

Therefore resistors with a resistance of 1 M Ω were soldered between the strips with a distance of 4.5mm and for the strips with 3 mm distance to the cathode respectively to the GEM a 666 k Ω resistor was used.

The last strip was soldered to a connector. This gives the possibility to variate the resistance before grounding the last strip, which in turn allows altering the potential

between last strip and GEM to match the drift field at this point. In figure 2.5 the completely mounted detector is shown.

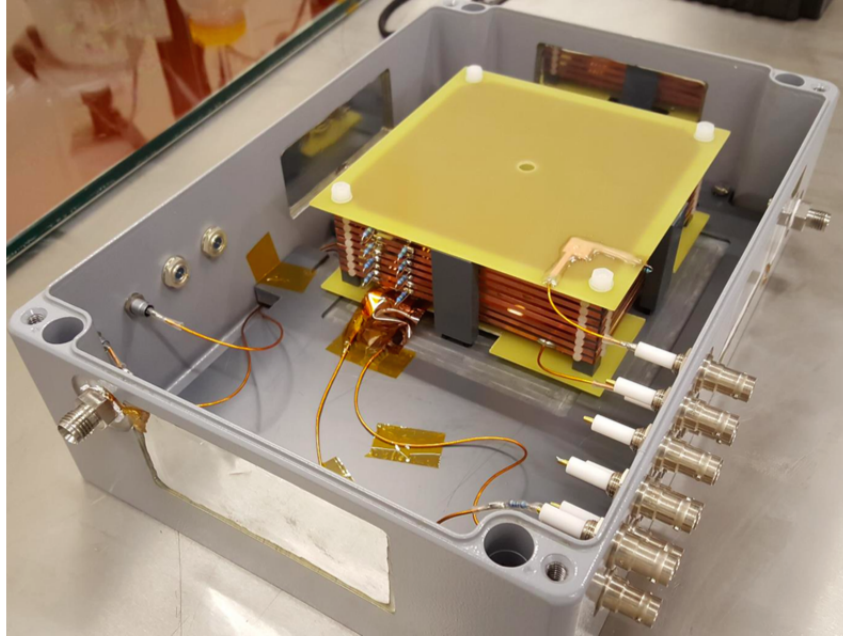


Figure 2.5: Completely mounted detector consisting readout anode, GEM, cathode and field cage with resistor chain

Chapter 3

Detector commissioning

This chapter gives an overview of the experimental setup. It focuses on the used gas and sources, their rates and the high voltage setting as well as the components of the readout system. Finally the spectrum of the sources are presented.

3.1 HV settings

The drift field is set to 400 V/cm whereas the induction field, determined as field between GEM bottom side and anode, is set to 3000 V/cm. This configuration is used in the ALICE TPC as well. This two values correspond to the scaling factor of 100%. Leaving the drift field constant to 400 V/cm and by altering the scaling factor, which scales or multiplies the GEM voltage and induction field, the fields can be varied leaving the ratio the same. In figure 3.1 the HV settings for the scaling factor from 90 % up to 110 % is shown.

Scaling factor (%)	Cathode voltage (V)	GEM voltage (V)	Induction field (V/cm)
110	2780	1100	3300
108	2760	1080	3240
106	2740	1060	3180
104	2720	1040	3120
102	2700	1020	3060
100	2680	1000	3000
98	2660	980	2940
96	2640	960	2880
94	2620	940	2820
92	2600	920	2760
90	2580	900	2700

Figure 3.1: HV settings for different scaling factors

3.2 Readout system

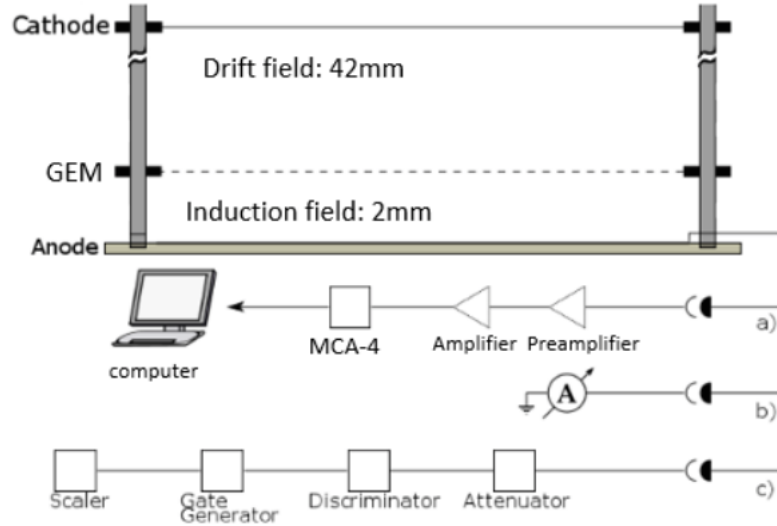


Figure 3.2: Schematic picture of a typical setup used for the gain and discharge probability studies. Different letters indicate possible chains to read out the anode signal.

The schematic readout system for rate and gain measurements is shown in figure 3.2 a). The raw signal induced at the anode is amplified by a charge sensitive preamplifier and is then processed to a timing amplifier where the signal is again amplified and also shaped. The next module in line is the MCA-4, which is a software controlled Multichannel Analyzer and sends the modified signal to the corresponding software on the computer where the signal can be examined. However, the gain is measured via the ratio of primary ionization current to the current measured at the pad plane, described in figure 3.2 b).

The latter is measured with a very precise ampere meter. The primary ionization current is calculated from the following formula:

$$I_{primary\ e^-} = R \cdot e \cdot N_{primary\ e^-} \quad (3.1)$$

The components of the formula are introduced in section 4.1. In case of discharge measurements (see fig. 3.2 c)), the signals do not need to be amplified due to the high energy released during the discharge. The raw signal induced on the pad plane is attenuated and then directed into the discriminator unit where the threshold is

set to -1 V. Only if the signal is above the threshold a signal is sent to the Gate Generator to filter out lower signals, which are not induced by discharges. To avoid multi-counting of the same signal, a gate of 1.2 s is created when the discriminator threshold is exceeded which is then counted by a scaler. [25] Figure 3.3 shows a typical signal of an electric spark.

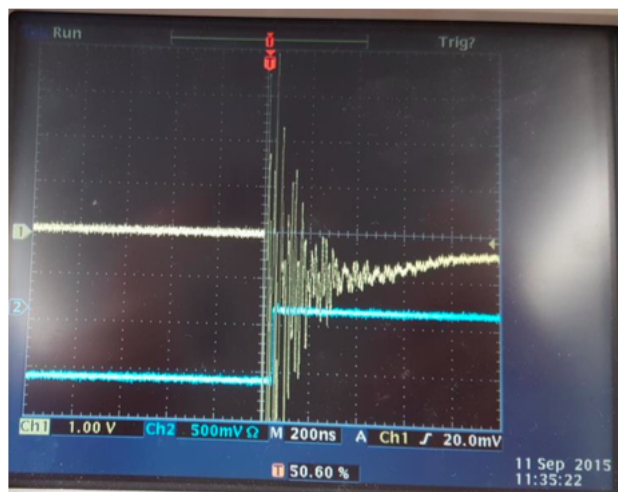


Figure 3.3: A typical signal associated with a spark in a small prototype, recorded by the oscilloscope. The blue channel shows the gate of 1.2 s.

3.3 Gas mixture

All the measurements are done in Ar-CO₂ with a ratio of 90-10. Argon is a so called noble gas and is quenched with carbon dioxide.

Due to the photon feedback, quenchers are mainly added for stability reasons. During amplification gas atoms get excited and de-excite again by emitting photons which can subsequently ionize or extract electrons from the surrounding electrodes. This effect is called photoelectric effect and can lead to deterioration of energy resolution and wrong track reconstruction, since avalanches could develop on random position. [27] Due to numerous vibrational and rotational excitation levels, quenchers are very likely to absorb photons therefore they are added.

In order to be able to calculate the primary currents, which is needed for gain

measurements, one have to calculate the effective ionization potential W_I . It is the energy, which is needed on average to create an electron ion pair in the gas. It can be easily calculated for gas mixtures with the W_I values for pure gases and the formula:

$$W_{I,n} = \frac{\sum_i x_i \cdot W_i}{\sum_i x_i} \quad (3.2)$$

Where x_i is the fraction of the gas I with the effective ionization potential W_i [25]. For ArCO₂ (90-10) the effective ionization potential is determined as 27.19 V.

3.4 Sources

There were two different radioactive sources used for the measurements. The ⁵⁵Fe source was used for gain measurements of the detector. Due to interaction with the gas molecules via photoelectric absorption followed by emitting photoelectrons, the full energy will be deposited in the sensitive gas volume. The ⁵⁵Fe source is a γ -source that emits photons with an energy of $E_\gamma = 5.89$ keV. [28]

Since all measurements were done in Ar-CO₂ (90-10), a second peak appeared in the spectrum. This peak is usually called single escape peak. It occurs due to photons ionizing electrons of the K-shell with the required amount of energy then followed by a de-excitation emitting photons leaving the active detector volume. The energy of the single escape peak in argon is $E_{\gamma, escape} = 2.89$ keV thus not the full energy is deposited. [29]

For discharge measurements a gaseous ²²⁰Rn source was used. ²²⁰Rn is an intermediate decay product of ²³²Th. By emitting an alpha particle, ⁴He nucleus, ²²⁰Rn decays to ²¹⁶Po with an energy of $E_{\alpha, Rn} = 6.29$ MeV. [28]

3.5 Rate determination

For identifying the rate, one uses the equation

$$R = \frac{N_{counts}}{t} \quad (3.3)$$

Where N_{counts} is the number of counts and t is the data acquisition time. It is important to mention that the acquisition time is referred to the live time, where actively data is processed and converted to a digital signal. In contrast to dead time, where data is lost, mainly due to the introduction of the logic gate. Moreover, the rates were measured while shooting with the source through the hole in the cathode in the case of ⁵⁵Fe or by connecting the gas pipe in line to the gaseous source of

^{220}Rn . By assuming that N_{counts} follows a Poisson distribution, only the error in N_{counts} need to be considered to estimate the error.

$$\Delta N_{counts} = \sqrt{N_{counts}} \quad (3.4)$$

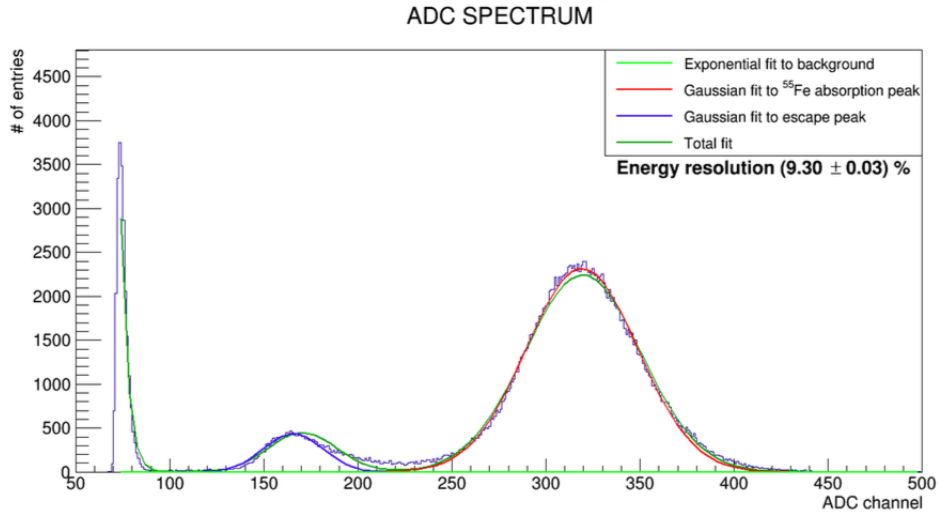
3.5.1 ^{220}Rn source

To define the rate of the ^{220}Rn source the signals in the ADC spectrum were counted and as mostly used in all measurements a data acquisition time of $t = 200$ s was chosen to measure the counts. Since the ^{220}Rn signals saturate the electronics when no attenuation is used the corresponding signals can be easily distinguished from the background signals. This leads to a rate of $R_{^{220}\text{Rn}} = (16.7 \pm 0.3)$ Hz. To determine the error of the rate only statistical uncertainty was taken to account since systematical uncertainty was very hard to distinguish. In addition, including systematical uncertainty would only shift the error bars in the plot, but it has no influence to the comparison of discharge probability of large pitch and standard foil, see section

3.5.2 ^{55}Fe source

To identify the rate of ^{55}Fe the readout scheme as explained in section 3.2 was used. As one can surly notice, the single escape peak appears before the full energy peak due to its lower energy and has a smaller amplitude since it is not as likely. (see fig. 3.4)

In order to determine the rate, the background is fitted with an exponential and subtracted from the data. In addition the ^{55}Fe absorption peak and the single escape peak are fitted with a gaussian. In the next step, the remaining entries under the peaks are counted. It is important to mention, that the rate can differ between the different measurements since the source is placed outside of the detector and one has to position and adjust the source by eye. To guarantee precise measurements the rate was measured every time again when the source position was changed. However, the rate was always approximately $R_{^{55}\text{Fe}} \approx 1300$ Hz.

Figure 3.4: ADC spectrum of ⁵⁵Fe in ArCO₂

3.6 Energy resolution (ER)

In the following, the common definition when working with gaseous detectors is used, which can be written as

$$ER = \frac{\sigma}{\mu} \quad (3.5)$$

Where σ is the standard deviation, which can be extracted from the gaussian fit as done in the figure above and μ is the mean value of the peak. This two values give an energy resolution of $(9.30 \pm 0.03) \%$.

The energy resolution may be improved by lowering a content of the oxygen in the gas mixture (see Sec. 2.1 for more details). The current, rather high value, implies non perfect sealing of the gas vessel. This can be improved in the future by using additional sealing at the mylar windows, HV or gas connectors.

Chapter 4

Gain measurement

This chapter focuses on the effective gain measurement, therefore the definition is introduced and the error estimation is motivated. In addition to it, the measurement itself will be presented and finally discussed.

4.1 Definition

Gain is defined as the mean ratio of the signal amplitude of the primary ionization current to the signal amplitude of the current measured at the anode. [30] Since neither all of the primary electrons arrive the GEM holes, because they end up at the top side of the GEM and thus do not get amplified, nor all of the avalanche electrons reach the readout anode due to recombination at the bottom side of the GEM, the effective gain G_{eff} can be defined as

$$G_{eff} = \frac{I_{anode}}{I_{primary\ e^-}} \quad (4.1)$$

I_{anode} is the current measured at the anode and $I_{primary\ e^-}$ can be calculated with

$$I_{primary\ e^-} = N_{primary\ e^-} \cdot R \cdot e^- = \frac{E_\gamma}{W_I} \cdot R \cdot e^- \quad (4.2)$$

where R is the rate, described in section 3.5, and e^- the elementary charge. The number of primary electrons $N_{primary\ e^-}$ can be written as

$$N_{primary\ e^-} = \frac{E_\gamma}{W_I} \quad (4.3)$$

E_γ is the energy deposited in the active volume of the detector which is in case of the ^{55}Fe source in Ar-based mixture is 5.89 keV for the full energy and 2.89 keV for the single escape peak, introduced in section 3.3.

4.2 Gain calculations and error estimation

First of all it should be noticed that gain dramatically depends on the density of the detector gas and thus on the ratio of temperature over pressure variations therefore before every new gain measurement was done the gain calibration was repeated.

The primary ionization current can be easily calculated by using equation 4.2. Whereas the current of the anode was directly measured by connecting the readout anode to an ampere meter. The scaling factor were varied from 90% up to 119%. Since the values of current were not stored but read off by eye, it has the highest influence on the error estimation. Considering the I_{anode} is in the range of nA, the error has been estimated to ± 0.002 nA. In addition to that, one has to involve the error caused by rate determination since the gain depends on the rate as well due to primary ionization current. The full error results in the error propagation of these two components. By using equation 4.1 gain can be calculated, which can be seen in the figures below.

The first gain measurement was done with the standard GEM foil as described above. Due to the high dependence of gain to pressure and temperature these values were noticed before every measurement. The pressure of the vicinity was in the first measurement 958.2 hPa and temperature was 22.6 C. The overpressure in the box due to constant gas flux was determined as 5.0 mbar and the O₂ content was 56.13 ppm.

In the second measurement implemented with the large pitch GEM foil, the pressure of the ambiance was determined as 964.9 hPa whereas the temperature was 22.3 C. Moreover, the overpressure was in the box 4.0 mbar and the O₂ content was 69.76 ppm.

The results of the gain measurement of both setup can be seen in the figures 4.1 and 4.2.

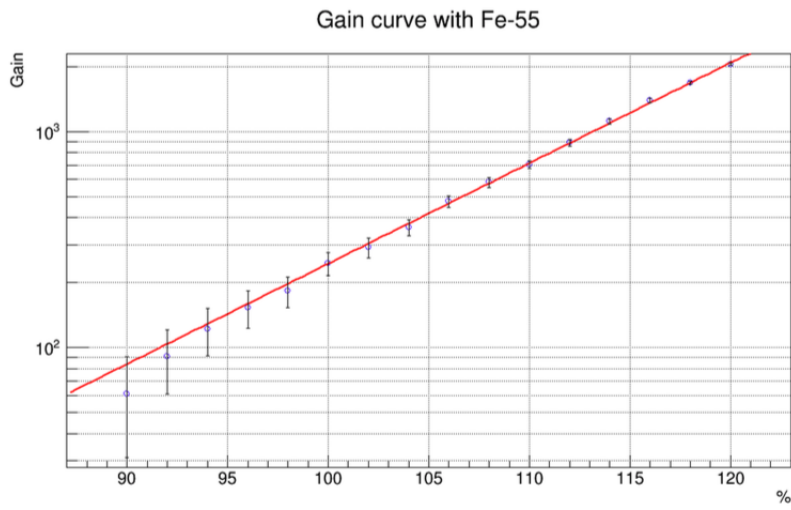


Figure 4.1: Gain plotted against the scaling factor with a logarithmic y-scale measured with standard GEM foil.

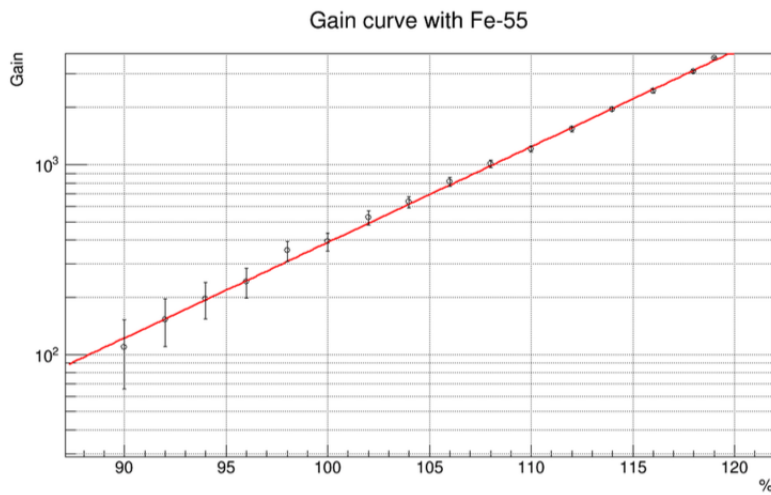


Figure 4.2: Gain plotted against the scaling factor with a logarithmic y-scale with large pitch GEM foil.

Chapter 5

Discharge studies

In the following chapter the definition of the discharge probability is presented. Moreover, the final results and error estimation is shown and compared to the published data of the *Technical Design Report for Upgrade of the ALICE Time Projection Chamber* [25].

5.1 Definition

In all measurements, the discharge probability is defined by the ratio of the discharge rate to the source rate

$$P_{dis} = \frac{N_{dis}}{t \cdot R} \quad (5.1)$$

Where $\frac{N_{dis}}{t}$ is the discharge rate measured by the number of electric sparks N_{dis} within the measurement time t , whereas R is the rate of the used radioactive source [25]. Assuming that the measured value N_{dis} follows a Poisson distribution, the statistical uncertainty can be estimated by

$$\Delta N_{dis} = \sqrt{N_{dis}} \quad (5.2)$$

The uncertainty in the rate of the alpha source has been given in subsection 3.5.1. Therefore the total statistical error of this quantity is calculated from error propagation and can be written as

$$\Delta P_{dis} = \frac{N}{t \cdot R} \sqrt{\left(\frac{\sqrt{N_{dis}}}{N_{dis}}\right)^2 + \left(\frac{\Delta R}{R}\right)^2} \quad (5.3)$$

The rate of the ^{220}Rn source were measured by integrating the energy spectrum after subtracting the background.

5.2 Results and comparison to the TDR addendum

The discharges were measured by using the readout scheme as described in section 3.2. The results are shown in figure 5.1. The discharge probability is plotted against

gain using two different detector setup.

The blue dots show the discharge probability of a standard foil whereas the red dots show the results of a large pitch foil. It is important to mention that the red dot around a gain of 240 only expresses an upper limit marked by the red arrow.

Due to the twice bigger hole pitch size of the large pitch foil and hence to a lower number of holes, the average charge density normalized to one hole is twice higher than in standard foils. Therefore the discharge probability is expected to be higher than for standard foils. Comparing this assumption to the results it is very hard to observe the effect of the pitch size within the errors on gain and discharge probability.

Still it is possible to discern discharge probability of large pitch foil being higher by a maximum factor of 2. Bigger differences would point to some defect in foils. To summarize the results, discharge probability is influenced by many effects and the pitch size may only have a minor influence.

To compare the measured results of the standard foil to the goal values from the TDR addendum it is important to notice that both detector setup conformed except that the drift gap used in the experiment published in the TDR addendum is 33 mm and no field cage was in the setup concluded. For all dimensions of the setup used for the experiment described in the thesis see section 2.2.

The results are in a fairly good agreement with the literature values. Despite that, the reference points are a bit shifted towards higher gains, which can be explained by the difference in the drift field. Since the drift field is 9 mm longer more electrons can be produced in the active detector volume and thus lead to discharge probability within lower gain.

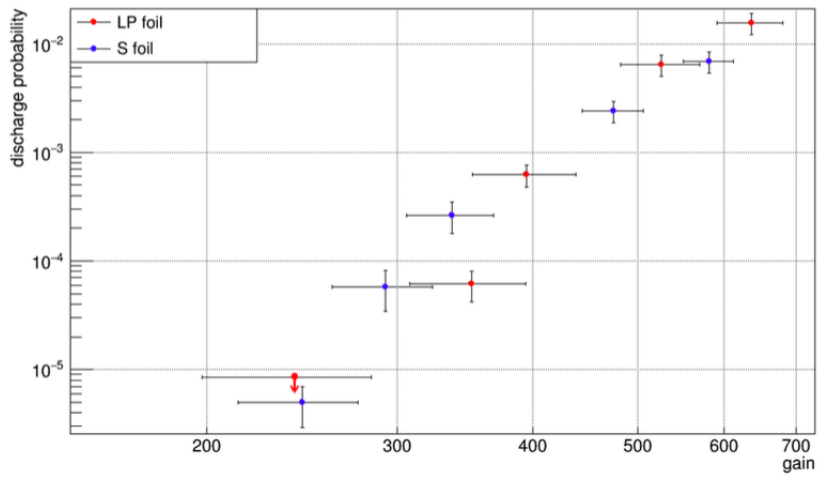


Figure 5.1: Discharge probability measured in a single GEM setup with a gaseous ^{220}Rn source in ArCO_2 (90-10)

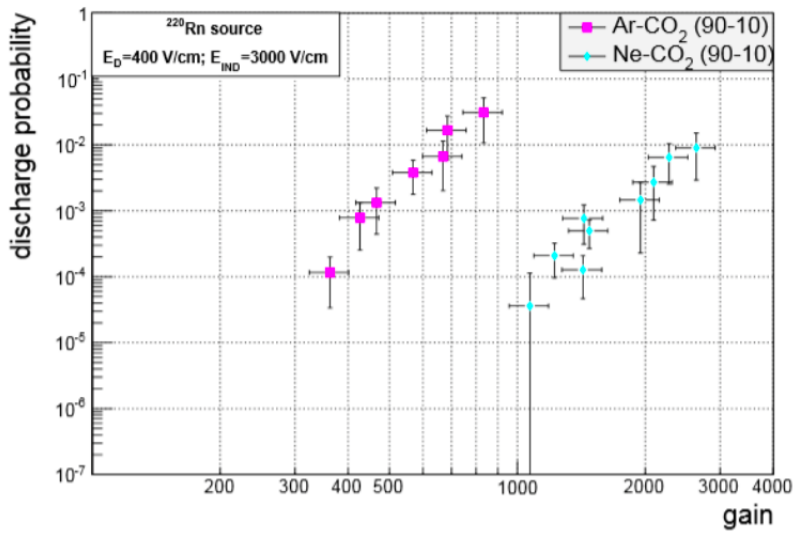


Figure 5.2: Reference data of the *Technical Design Report for Upgrade of the ALICE Time Projection Chamber* citetwentyfour

Chapter 6

Summary & Outlook

6.1 Summary

This work has been carried out in the framework of the ALICE TPC upgrade collaboration.

The goal of this work was the commissioning of a small prototype detector with field cage and the study of discharge probability in order to achieve the goal values, which are published in the *Technical Design Report for the Upgrade of the ALICE Time Projection Chamber*.

Therefore a new GEM prototype detector was designed in solid works including a field cage to homogenize the drift field. In an already existing laboratory environment the new detector setup was tested by comparing the expected current to the current flowing through the cathode and the resistor chain of the field cage. This showed that the detector was perfectly running just after commissioning.

In a first study the rate of the used sources and the energy resolution was determined. Within a second study a dedicated investigation of the amplification behavior of a single GEM setup with a large pitch foil and a standard foil was measured. This was necessary to provide precise results of the discharge probability comparing properties against electric sparks of standard and large pitch foil.

It occurred that discharge probability is a very complex effect and it is hard to observe the effect of the pitch size within the errors on gain and discharge probability. However, comparing the final results it exposed that discharge probability emphasized to be higher than for standard foils with a maximum factor of 2.

In addition to that a detailed study and reference was realized. Furthermore, this thesis focused on the relevant error estimation for gain and discharge measurements. In terms of all measurements, it was possible to achieve the goal values for discharge probability referred to the TDR addendum.

6.2 Outlook

Further investigation is still needed not only to identify the above mentioned effects but also to fully understand the characteristics of discharges.

First step is to improve the tightness of the detector since the oxygen level saturated around 60 ppm. To obtain very precise results concerning discharge probability it is very important to have the lowest possible oxygen content since this is a quencher and could distort the results.

Since this thesis focused on the difference between standard and large pitch foil concerning discharge probability the first time, it could be also interesting to do more experiments altering e.g. the T/p variation or gas mixtures to study discharge effects. Another possibility could be to use the detector setup with field cage to study gain and discharge probability with multi GEM stacks.

Next step could be to test the detector setup on the MLL laboratory (Maier Leibnitz Laboratory) with protons or ions since the detector box was designed to have the possibility to shoot with a beam. Since the ALICE TPC uses a field cage to ensure the uniformity of the electric field as well, better approximations could be estimated to optimize the settings used for GEM detectors.

Appendix A

Oscilloscope signals

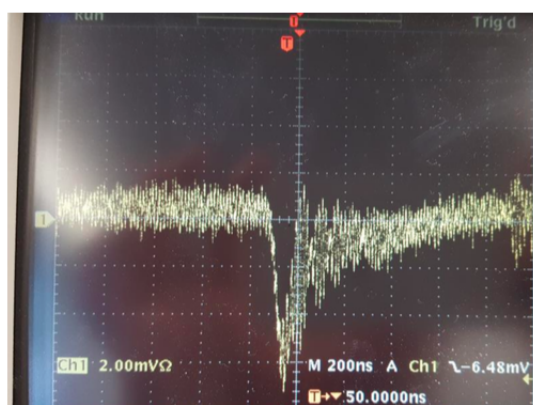


Figure A.1: Raw signal of a ^{55}Fe source

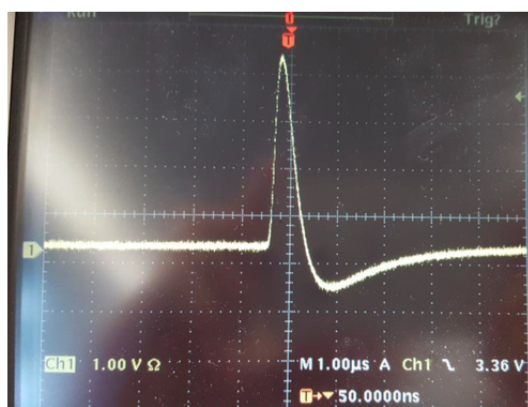


Figure A.2: Shaped and amplified signal of ^{55}Fe source

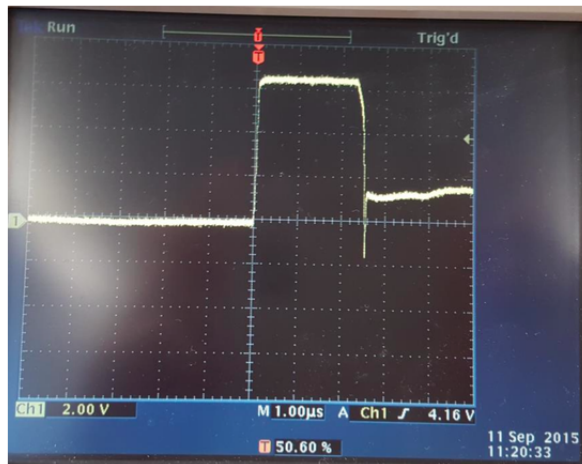


Figure A.3: Shaped and amplified signal of ^{220}Rn source

Bibliography

- [1] J. Rafelski; B. Müller. *Strangeness Production in the Quark-Gluon Plasma*. Phys. Rev. Lett. 56, S. 2334., 1999.
- [2] A. Ipp. 2002. URL: <http://hep.itp.tuwien.ac.at/~ipp/imagesphysics01/QGM.jpg>.
- [3] J. Alme. *The Alice tpc, a large 3-dimensional tracking device with fast readout for ultra-high multiplicity events*. Nucl. Inst. Meth. Phys. Res., 622:316, 2010.
- [4] GEM-TPC Collaboration. *Technical Design Study for the PANDA Time Projection Chamber*. 2012.
- [5] W. R. Leo. *Techniques for Nuclear and Particle Physics Experiments*. Springer, Second Edition, 2009.
- [6] S. Afanasiev. *Nucl. Instr. and Meth. A* 430. 1999.
- [7] G. Charpak. *NIM* 62, 262. 1968.
- [8] LC TPC. 2015. URL: <http://www.lctpc.org/e8/e57671/>.
- [9] ALICE TPC collaboration. *Technical design report of the Alice tpc upgrade*. 2013.
- [10] C. Garabatos. *Nucl. Instr. and Meth. A* 535. 2004.
- [11] F. Sauli. *Nucl. Instr. and Meth. A* 386, 531. 1997.
- [12] G. Knoll. *Radiation Detection and Measurement*. 2nd ed. New York: Willey, 1989.
- [13] H. J. Hilke. *Time Projection Chambers*. Rep. Prog. Phys., 73:116201, 2010.
- [14] F. Sauli. *Gem: A new concept for electron amplification in gas detectors*. Nucl. Instr. Meth. A, 1997.
- [15] A. Augustinus; M. Berger; F. Böhmer; F. Carena; S. Dorheim; J. Hehner; H. D. Hernandez; A. Jusko; M. Krivda; P. Martinengo; A. D. Mauro; T. Morhardt; R. Oliveira; E. Oliveri; F. Raviel; L. Ropelewski; G. Scioli; M. V. Stenis; A. Tauro; A. Wasem. *Upgrade of the ALICE Time Projection Chamber*. CERN-LHCC-2013-020 / ALICE-TDR- 016.
- [16] L. Fabbietti; B. Ketzner. *Technical Design Study for the PANDA Time Projection Chamber*. 2012.

- [17] P. Abb. *The compass experiment at cern*. Nucl. Instr. Meth. A, 557:455-518, 1997.
- [18] B. Ketzer. *Performance of triple gem tracking detectors in the compass experiment*. Nucl. Instr. Meth. A, 535:314-318, 2004.
- [19] L. Fabbietti. *The panda gem-based tp c prototyp*. Nucl. Instr. Meth. A, 628:204-208, 2011.
- [20] C. Schwarz. *The panda experiment*. J. Phys.: Conf. Ser. , 374, 2012.
- [21] V. Peskov; P. Fonte. *Research on discharges in micropattern and small gap gaseous detectors*. 2009.
- [22] H. Raether. *Electron avalanches and breakdown in gases*. Butterworths, 1964.
- [23] Yu. Ivanououchenkov. *Nucl. Instr. and Meth. A 422, 300*. 1999.
- [24] P. Fonte. *Nucl. Instr. and Meth. A 416, 23*. 1998.
- [25] The ALICE Collaboration. *Addendum to the Technical Design Report for the Upgrade of the ALICE Time Projection Chamber*. ALICE-TDR-016-ADD-1, 2015.
- [26] *Technical Alerts News SolidWorks*. Jul 31, 2015.
- [27] F. Haas. *Moderne Detektoren für die Kern- und Teilchenphysik*. lecture, 2014.
- [28] PDG. 2014. URL: <http://pdg.lbl.gov/>.
- [29] T. Sinha; D. Das; S. Chattopadhyay; S. Bose. *Study on the performance of a single-THGEM gas detector*. Proceedings of the DAE Symp. on Nucl. Phys. 55, 2010.
- [30] F. R. Graf. *Modern Dictionary of Electronics (7 ed.)* Newnes, 1999.

Acknowledgements

First of all, I would like to thank Prof. Laura Fabbietti for giving me the great opportunity and making this thesis possible. I also want to thank her for her outstanding motivational spirit and the brilliant input she provided. I would also like to thank for her confidence and trust to allow building a detector by myself.

I am most thankful to my supervisor Dr. Piotr Gasik who not only taught me a lot about particle detection and the underlying physics in his lecture on gaseous detectors but also supported me. Regarding his inspiring motivation and deep knowledge of experimental physics, I am very thankful for his involvement in my work.

I would like to thank Andreas Mathis for lending me his support and motivation in every situation I was stucked. I really enjoyed working with him together.

I also want to thank Robert Mnzer for his help in the GEM laboratory and the very interesting lecture he was giving too. I want to thank Petra Mschenborn to teach and helped my soldering.

I want to thank Ralf Lang who was an incredible help designing the detector.

Special thanks go to my loving parents for their support and motivating words. Overall I want to thank Gramos Qerimi who is not only my love but also my fellow student and although he was just as busy as I, he always believed and supported me.